

Semi-implicit Lax-Wendroff kinetic scheme for electron–phonon coupling

Jiaming Li^a, Hong Liang^{a,*}, Meng Lian^b, Chuang Zhang^{c,*}, Jiangrong Xu^{a,d}

^a*Department of Physics, Hangzhou Dianzi University, Hangzhou 310018, China*

^b*School of Physics, Institute for Quantum Science and Engineering and Wuhan National High Magnetic Field Center,*

Huazhong University of Science and Technology, Wuhan 430074, China

^c*College of Energy Engineering, Zhejiang University, Hangzhou 310027, China*

^d*College of Energy Environment and Safety Engineering, China Jiliang University, Hangzhou 310018, China*

Abstract

A semi-implicit Lax-Wendroff scheme is developed for electron-phonon coupling process in metals based on the two-temperature kinetic equations. The core of this method is to integrate the evolution information of physical equations into the numerical modeling process, which leads to that the time step or cell size is not limited by the relaxation time and mean free path. Specifically, the finite difference method is used to solve the kinetic model again when reconstructing the interfacial distribution function, through which the particle migration, scattering and electron-phonon coupling processes are coupled together within a single time step. Numerical tests demonstrate that this method could efficiently capture electron-phonon coupling or heat conduction processes from the ballistic to diffusive regimes. It provides a new tool for describing electron–phonon coupling or thermal management in microelectronic devices.

Keywords: Electron–phonon coupling, Multi-scale heat conduction, Boltzmann transport equation, Semi-implicit Lax-Wendroff kinetic scheme

1. Introduction

As the Moore’s Law of chips gradually approaches its physical limit [1, 2] and breakthroughs in packaging or laser technology prompt a transition from the millimeter or second scales to the nanometer or ultra-fast time scales, non-equilibrium thermal transport has become a key frontier foundation in the industrialization process [3, 4, 5, 6, 7, 8]. At the micro/nano scales, the mean free path or relaxation time of thermal carriers (e.g., electron and phonon) is comparable to the characteristic length or time scale of the system and the classical Fourier heat conduction theory fails, which necessitates a fundamental shift toward characterizing non-equilibrium transport and scattering of thermal carriers [9, 10] as the primary determinant of device performance and lifespan. Consequently, understanding these transport and interactions mechanisms is the definitive bottleneck for advancing thermal management in next-generation electronics and precision laser machining [11, 12, 13, 14].

*Corresponding author

Email addresses: 780867508@qq.com (Jiaming Li), lianghongstefanie@163.com (Hong Liang), lianmeng@hust.edu.cn (Meng Lian), zhangc26@zju.edu.cn (Chuang Zhang), 21A3100028@cjlu.edu.cn (Jiangrong Xu)

Many theoretical models have been developed in the past to describe the fundamental electron-phonon coupling process [15, 16, 17, 18, 19, 20, 21]. The two-temperature model (TTM) proposed by Anisimov et al. [22], which describes coupled electron and phonon temperature fields through coupled diffusion equations, has become a useful and simple tool for scenarios like ultra-fast laser heating. But the limitations of traditional TTM become increasingly apparent for complex material systems. It neglects the thermal non-equilibrium between optical and acoustic phonon [23, 24, 25]. To address this, the non-thermal lattice model [20] or multi-temperature model [13] was developed, which more precisely describes energy relaxation pathways by establishing separate energy equations for electrons, optical phonon, and acoustic phonon. However, both the TTM and MTM rely on diffusion assumption, which neglects non-instantaneous nature of energy transfer [26] and fails to capture ballistic transport, nonlocal or nonlinear effects. Compared to the macroscopic models, the Boltzmann transport equation (BTE) provides a more fundamental theoretical framework for electron-phonon coupling [27, 28, 29, 30, 31]. The phonon/electron BTE naturally encompass carrier scattering, transport and coupling processes through distribution function evolution, enabling a unified description of thermal transport behavior from ballistic to diffusive regimes. This kinetic model provides a detailed description of non-equilibrium distributions, captures size effects, boundary scattering and self-consistently couples multi-carrier transport. However, the BTE is a high-dimensional integral-differential equation, posing significant challenges for analytical or numerical solutions.

Over the past decades, numerous numerical methods for solving the BTE have been developed [32, 33, 34], such as the lattice Boltzmann method [31, 35], explicit discrete ordinate method [29, 36] and Monte Carlo method [37]. These methods have played significant and successful roles at different scales. However, it is difficult for them to maintain extremely high computational efficiency and accuracy for all Knudsen numbers due to the introduction of some approximations or assumptions in numerical modeling process [38, 39]. The lattice Boltzmann method is unable to accurately describe the heat transfer phenomena in the highly non-equilibrium or ballistic regime due to the limited discrete points in the momentum space [35]. The latter two methods decouple the particle migration and scattering on a numerical time step scale. Therefore, the time step is limited by the relaxation time, making them difficult to efficiently simulate unsteady thermal transport problems with extremely small Knudsen numbers [40, 33, 34].

Recently, a semi-implicit Lax-Wendroff kinetic scheme has been developed for solving BTE [41], demonstrating its ability to capture transitions from ballistic to diffusive transient heat transfer and its independence from relaxation time constraints [42]. Given the excellent performance of this method in a single physical field [42, 41], this study further expands it and applies it to the multi-scale heat conduction problem with electron-phonon coupling. The rest of the paper is organized as follows. In Sec. 2, the kinetic model is introduced as well as the semi-implicit Lax-Wendroff scheme. Numerical simulations and tests are shown in Sec. 3. Conclusions are made in Sec. 4.

2. Model and Numerical Algorithm

2.1. Electron and Phonon BTE

The Boltzmann transport equation for electron-phonon coupling is expressed as follows [9, 32, 33, 27, 28, 29, 30, 31],

$$\frac{\partial f_e}{\partial t} + \mathbf{v}_e \cdot \nabla_{\mathbf{x}} f_e = \frac{1}{\tau_e} (f_e^{eq} - f_e) - \frac{G}{4\pi} (T_e - T_p), \quad (1)$$

$$\frac{\partial f_p}{\partial t} + \mathbf{v}_p \cdot \nabla_{\mathbf{x}} f_p = \frac{1}{\tau_p} (f_p^{eq} - f_p) + \frac{G}{4\pi} (T_e - T_p). \quad (2)$$

where the subscripts e and p represent electron and phonon, respectively. These subscripts will be consistently adopted throughout the remainder of this paper. The electron and phonon energy density distribution functions are given by $f_e = f_e(\mathbf{x}, \mathbf{v}_e, t)$ and $f_p = f_p(\mathbf{x}, \mathbf{v}_p, t)$, respectively, which depend on the spatial position \mathbf{x} , time t and group velocity $\mathbf{v}_e = |\mathbf{v}_e| \mathbf{s}$ or $\mathbf{v}_p = |\mathbf{v}_p| \mathbf{s}$. $\mathbf{s} = (\cos \theta, \sin \theta \cos \varphi, \sin \theta \sin \varphi)$ is the unit directional vector with polar angle θ and azimuthal angle φ . τ is the relaxation time and the electron-phonon coupling constant is denoted by G . The equilibrium distribution functions for electron and phonon are given as follows,

$$f_e^{eq} = \frac{C_e T_e}{4\pi}, \quad f_p^{eq} = \frac{C_p T_p}{4\pi}. \quad (3)$$

where C is the specific heat and T is the temperature. Energy conservation is satisfied during the electron-electron, phonon-phonon scattering processes,

$$\int \frac{f_e^{eq} - f_e}{\tau_e} d\Omega = 0, \quad \int \frac{f_p^{eq} - f_p}{\tau_p} d\Omega = 0. \quad (4)$$

where $d\Omega$ represents the integral over the whole solid angle space. Macroscopic variables including the local energy density U , heat flux \mathbf{q} and temperature T are obtained by taking the moment of distribution function.

$$U_e = \int f_e d\Omega, \quad q_e = \int v_e f_e d\Omega, \quad T_e = \frac{1}{C_e} \int f_e d\Omega = \frac{U_e}{C_e}, \quad (5)$$

$$U_p = \int f_p d\Omega, \quad q_p = \int v_p f_p d\Omega, \quad T_p = \frac{1}{C_p} \int f_p d\Omega = \frac{U_p}{C_p}. \quad (6)$$

2.2. Semi-implicit Lax-Wendroff kinetic scheme

The semi-implicit Lax-Wendroff kinetic scheme [41] is introduced for electron-phonon coupling in detail. Taking a two-dimensional kinetic model as an example for ease of understanding and keeping generality, the discretization process of the present scheme is,

$$\frac{\partial f_e}{\partial t} + u_e \frac{\partial f_e}{\partial x} + v_e \frac{\partial f_e}{\partial y} = \frac{1}{\tau_e} (f_e^{eq} - f_e) - \frac{G}{4\pi} (T_e - T_p), \quad (7)$$

$$\frac{\partial f_p}{\partial t} + u_p \frac{\partial f_p}{\partial x} + v_p \frac{\partial f_p}{\partial y} = \frac{1}{\tau_p} (f_p^{eq} - f_p) + \frac{G}{4\pi} (T_e - T_p), \quad (8)$$

where $u = |v| \cos \theta$ and $v = |v| \sin \theta \cos \varphi$ are the x -component and y -component of the group velocity, respectively. Uniform Cartesian grid is used for both the spatial and temporal spaces under the framework of finite volume method, where $(\Delta x, N_x, i)$ and $(\Delta y, N_y, j)$ are the (cell size, total cell number, index of cell center) in the x and y direction, respectively. The solid angle space is discretized with the index k , too.

Taking an integral of the governing equations over the time interval from t^n to $t^{n+1} = t^n + \Delta t$ for a controlled volume leads to,

$$\frac{f_{e,i,j,k}^{n+1} - f_{e,i,j,k}^n}{\Delta t} + u_{e,k} \frac{\partial f_{e,i,j,k}^{n+1/2}}{\partial x} + v_{e,k} \frac{\partial f_{e,i,j,k}^{n+1/2}}{\partial y} = \frac{1}{2} \left(\frac{f_{e,i,j,k}^{eq,n+1} - f_{e,i,j,k}^{n+1}}{\tau_e} + \frac{f_{e,i,j,k}^{eq,n} - f_{e,i,j,k}^n}{\tau_e} \right) - \frac{G}{8\pi} (T_{e,i,j}^{n+1} - T_{p,i,j}^{n+1} + T_{e,i,j}^n - T_{p,i,j}^n), \quad (9)$$

$$\frac{f_{p,i,j,k}^{n+1} - f_{p,i,j,k}^n}{\Delta t} + u_{p,k} \frac{\partial f_{p,i,j,k}^{n+1/2}}{\partial x} + v_{p,k} \frac{\partial f_{p,i,j,k}^{n+1/2}}{\partial y} = \frac{1}{2} \left(\frac{f_{p,i,j,k}^{eq,n+1} - f_{p,i,j,k}^{n+1}}{\tau_p} + \frac{f_{p,i,j,k}^{eq,n} - f_{p,i,j,k}^n}{\tau_p} \right) + \frac{G}{8\pi} (T_{e,i,j}^{n+1} - T_{p,i,j}^{n+1} + T_{e,i,j}^n - T_{p,i,j}^n), \quad (10)$$

where $f_{e,i,j,k}^n = f_e(x_i, y_j, u_{e,k}, v_{e,k}, t^n)$, $f_{p,i,j,k}^n = f_p(x_i, y_j, u_{p,k}, v_{p,k}, t^n)$. The right-hand sides of the above equation are discretized by the trapezoidal rule and the flux terms are handled via the midpoint rule. The spatial gradients of distribution function are

$$\frac{\partial f_{i,j,k}^{n+1/2}}{\partial x} = \frac{f_{i+1/2,j,k}^{n+1/2} - f_{i-1/2,j,k}^{n+1/2}}{\Delta x}, \quad \frac{\partial f_{i,j,k}^{n+1/2}}{\partial y} = \frac{f_{i,j+1/2,k}^{n+1/2} - f_{i,j-1/2,k}^{n+1/2}}{\Delta y}, \quad (11)$$

where $(i \pm 1/2, j)$ or $(i, j \pm 1/2)$ represents the indexes of cell interfaces connected to cell center (i, j) in the x - and y - direction, respectively.

Reformulating Eqs.(9,10),

$$f_{e,i,j,k}^{n+1} = \frac{\tau_e}{\tau_e + h} f_{e,i,j,k}^n + \frac{h}{\tau_e + h} f_{e,i,j,k}^{eq,n+1} + \frac{h}{\tau_e + h} (f_{e,i,j,k}^{eq,n} - f_{e,i,j,k}^n) - \frac{2h\tau_e}{\tau_e + h} \left(u_{e,k} \frac{f_{e,i+1/2,j,k}^{n+1/2} - f_{e,i-1/2,j,k}^{n+1/2}}{\Delta x} + v_{e,k} \frac{f_{e,i,j+1/2,k}^{n+1/2} - f_{e,i,j-1/2,k}^{n+1/2}}{\Delta y} \right) - \frac{h\tau_e}{\tau_e + h} \frac{G}{4\pi} (T_{e,i,j}^{n+1} - T_{p,i,j}^{n+1} + T_{e,i,j}^n - T_{p,i,j}^n), \quad (12)$$

$$f_{p,i,j,k}^{n+1} = \frac{\tau_p}{\tau_p + h} f_{p,i,j,k}^n + \frac{h}{\tau_p + h} f_{p,i,j,k}^{eq,n+1} + \frac{h}{\tau_p + h} (f_{p,i,j,k}^{eq,n} - f_{p,i,j,k}^n) - \frac{2h\tau_p}{\tau_p + h} \left(u_{p,k} \frac{f_{p,i+1/2,j,k}^{n+1/2} - f_{p,i-1/2,j,k}^{n+1/2}}{\Delta x} + v_{p,k} \frac{f_{p,i,j+1/2,k}^{n+1/2} - f_{p,i,j-1/2,k}^{n+1/2}}{\Delta y} \right) + \frac{h\tau_p}{\tau_p + h} \frac{G}{4\pi} (T_{e,i,j}^{n+1} - T_{p,i,j}^{n+1} + T_{e,i,j}^n - T_{p,i,j}^n), \quad (13)$$

where $h = \Delta t/2$. Taking the moment of Eqs.(9,10) leads to the macroscopic governing equation at the cell center,

$$U_{e,i,j}^{n+1} = U_{e,i,j}^n - \Delta t \sum_k \left(u_{e,k} \frac{f_{e,i+1/2,j,k}^{n+1/2} - f_{e,i-1/2,j,k}^{n+1/2}}{\Delta x} + v_{e,k} \frac{f_{e,i,j+1/2,k}^{n+1/2} - f_{e,i,j-1/2,k}^{n+1/2}}{\Delta y} \right) \phi_k - hG (T_{e,i,j}^{n+1} - T_{p,i,j}^{n+1} + T_{e,i,j}^n - T_{p,i,j}^n), \quad (14)$$

$$U_{p,i,j}^{n+1} = U_{p,i,j}^n - \Delta t \sum_k \left(u_{p,k} \frac{f_{p,i+1/2,j,k}^{n+1/2} - f_{p,i-1/2,j,k}^{n+1/2}}{\Delta x} + v_{p,k} \frac{f_{p,i,j+1/2,k}^{n+1/2} - f_{p,i,j-1/2,k}^{n+1/2}}{\Delta y} \right) \phi_k + hG (T_{e,i,j}^{n+1} - T_{p,i,j}^{n+1} + T_{e,i,j}^n - T_{p,i,j}^n), \quad (15)$$

where \sum_k is the numerical quadrature over the discretized solid angle space and ϕ_k is the associated weight.

Based on Eqs.(3,5,6), the equilibrium state is completely determined by the local temperature or energy density. Combining the above two equations (14,15) yields a system of two linear equations in two variables concerning electron and phonon temperatures at the next time step. Therefore, the key step is calculating the unknown electron and phonon distribution functions at the cell interfaces at the half-time step ($t^{n+1/2}$). Taking an integral of the BTE from t^n to $t^{n+1/2} = t^n + h$ at the cell interfaces $(x_{i+1/2}, y_j)$ and $(x_i, y_{j+1/2})$ leads to,

$$\frac{f_{e,i+1/2,j,k}^{n+1/2} - f_{e,i+1/2,j,k}^n}{h} + u_{e,k} \frac{\partial f_{e,i+1/2,j,k}^n}{\partial x} + v_{e,k} \frac{\partial f_{e,i+1/2,j,k}^n}{\partial y} = \frac{1}{\tau_e} (f_{e,i+1/2,j,k}^{eq,n+1/2} - f_{e,i+1/2,j,k}^{n+1/2}) - \frac{G}{4\pi} (T_{e,i+1/2,j}^{n+1/2} - T_{p,i+1/2,j}^{n+1/2}), \quad (16)$$

$$\frac{f_{e,i,j+1/2,k}^{n+1/2} - f_{e,i,j+1/2,k}^n}{h} + u_{e,k} \frac{\partial f_{e,i,j+1/2,k}^n}{\partial x} + v_{e,k} \frac{\partial f_{e,i,j+1/2,k}^n}{\partial y} = \frac{1}{\tau_e} (f_{e,i,j+1/2,k}^{eq,n+1/2} - f_{e,i,j+1/2,k}^{n+1/2}) - \frac{G}{4\pi} (T_{e,i,j+1/2}^{n+1/2} - T_{p,i,j+1/2}^{n+1/2}), \quad (17)$$

$$\frac{f_{p,i+1/2,j,k}^{n+1/2} - f_{p,i+1/2,j,k}^n}{h} + u_{p,k} \frac{\partial f_{p,i+1/2,j,k}^n}{\partial x} + v_{p,k} \frac{\partial f_{p,i+1/2,j,k}^n}{\partial y} = \frac{1}{\tau_p} (f_{p,i+1/2,j,k}^{eq,n+1/2} - f_{p,i+1/2,j,k}^{n+1/2}) + \frac{G}{4\pi} (T_{e,i+1/2,j}^{n+1/2} - T_{p,i+1/2,j}^{n+1/2}), \quad (18)$$

$$\frac{f_{p,i,j+1/2,k}^{n+1/2} - f_{p,i,j+1/2,k}^n}{h} + u_{p,k} \frac{\partial f_{p,i,j+1/2,k}^n}{\partial x} + v_{p,k} \frac{\partial f_{p,i,j+1/2,k}^n}{\partial y} = \frac{1}{\tau_p} (f_{p,i,j+1/2,k}^{eq,n+1/2} - f_{p,i,j+1/2,k}^{n+1/2}) + \frac{G}{4\pi} (T_{e,i,j+1/2}^{n+1/2} - T_{p,i,j+1/2}^{n+1/2}), \quad (19)$$

where the right-hand sides of the above equation are discretized by the forward-Euler rule and the flux terms are handled via the backward-Euler rule. Making a transformation of above equations leads to,

$$f_{e,i+1/2,j,k}^{n+1/2} = \frac{\tau_e}{\tau_e + h} f_{e,i+1/2,j,k}^n - \frac{\tau_e h}{\tau_e + h} \left(u_{e,k} \frac{\partial f_{e,i+1/2,j,k}^n}{\partial x} + v_{e,k} \frac{\partial f_{e,i+1/2,j,k}^n}{\partial y} \right) + \frac{h}{\tau_e + h} f_{e,i+1/2,j,k}^{eq,n+1/2} - \frac{\tau_e h}{\tau_e + h} \frac{G}{4\pi} (T_{e,i+1/2,j}^{n+1/2} - T_{p,i+1/2,j}^{n+1/2}), \quad (20)$$

$$\begin{aligned}
f_{e,i,j+1/2,k}^{n+1/2} &= \frac{\tau_e}{\tau_e + h} f_{e,i,j+1/2,k}^n - \frac{\tau_e h}{\tau_e + h} \left(u_{e,k} \frac{\partial f_{e,i,j+1/2,k}^n}{\partial x} + v_{e,k} \frac{\partial f_{e,i,j+1/2,k}^n}{\partial y} \right) + \frac{h}{\tau_e + h} f_{e,i,j+1/2,k}^{eq,n+1/2} \\
&\quad - \frac{\tau_e h}{\tau_e + h} \frac{G}{4\pi} (T_{e,i,j+1/2}^{n+1/2} - T_{p,i,j+1/2}^{n+1/2}),
\end{aligned} \tag{21}$$

$$\begin{aligned}
f_{p,i+1/2,j,k}^{n+1/2} &= \frac{\tau_p}{\tau_p + h} f_{p,i+1/2,j,k}^n - \frac{\tau_p h}{\tau_p + h} \left(u_{p,k} \frac{\partial f_{p,i+1/2,j,k}^n}{\partial x} + v_{p,k} \frac{\partial f_{p,i+1/2,j,k}^n}{\partial y} \right) + \frac{h}{\tau_p + h} f_{p,i+1/2,j,k}^{eq,n+1/2} \\
&\quad + \frac{\tau_p h}{\tau_p + h} \frac{G}{4\pi} (T_{e,i+1/2,j}^{n+1/2} - T_{p,i+1/2,j}^{n+1/2}),
\end{aligned} \tag{22}$$

$$\begin{aligned}
f_{p,i,j+1/2,k}^{n+1/2} &= \frac{\tau_p}{\tau_p + h} f_{p,i,j+1/2,k}^n - \frac{\tau_p h}{\tau_p + h} \left(u_{p,k} \frac{\partial f_{p,i,j+1/2,k}^n}{\partial x} + v_{p,k} \frac{\partial f_{p,i,j+1/2,k}^n}{\partial y} \right) + \frac{h}{\tau_p + h} f_{p,i,j+1/2,k}^{eq,n+1/2} \\
&\quad + \frac{\tau_p h}{\tau_p + h} \frac{G}{4\pi} (T_{e,i,j+1/2}^{n+1/2} - T_{p,i,j+1/2}^{n+1/2}),
\end{aligned} \tag{23}$$

Taking the moment of Eqs.(24,25,26,27) leads to the macroscopic governing equation at the cell interface,

$$U_{e,i+1/2,j}^{n+1/2} = U_{e,i+1/2,j}^n - h \sum_k \left(u_{e,k} \frac{\partial f_{e,i+1/2,j,k}^n}{\partial x} + v_{e,k} \frac{\partial f_{e,i+1/2,j,k}^n}{\partial y} \right) \phi_k - hG (T_{e,i+1/2,j}^{n+1/2} - T_{p,i+1/2,j}^{n+1/2}), \tag{24}$$

$$U_{e,i,j+1/2}^{n+1/2} = U_{e,i,j+1/2}^n - h \sum_k \left(u_{e,k} \frac{\partial f_{e,i,j+1/2,k}^n}{\partial x} + v_{e,k} \frac{\partial f_{e,i,j+1/2,k}^n}{\partial y} \right) \phi_k - hG (T_{e,i,j+1/2}^{n+1/2} - T_{p,i,j+1/2}^{n+1/2}), \tag{25}$$

$$U_{p,i+1/2,j}^{n+1/2} = U_{p,i+1/2,j}^n - h \sum_k \left(u_{p,k} \frac{\partial f_{p,i+1/2,j,k}^n}{\partial x} + v_{p,k} \frac{\partial f_{p,i+1/2,j,k}^n}{\partial y} \right) \phi_k + hG (T_{e,i+1/2,j}^{n+1/2} - T_{p,i+1/2,j}^{n+1/2}), \tag{26}$$

$$U_{p,i,j+1/2}^{n+1/2} = U_{p,i,j+1/2}^n - h \sum_k \left(u_{p,k} \frac{\partial f_{p,i,j+1/2,k}^n}{\partial x} + v_{p,k} \frac{\partial f_{p,i,j+1/2,k}^n}{\partial y} \right) \phi_k + hG (T_{e,i,j+1/2}^{n+1/2} - T_{p,i,j+1/2}^{n+1/2}). \tag{27}$$

In order to obtain $U^{n+1/2}$ or $T^{n+1/2}$, it is inevitable is to calculate the interfacial distribution function and its spatial gradients at the n -time step (t^n) based on above four equations. Fortunately, the detailed calculation formula of interfacial distribution function and its spatial gradients has been written in the previous paper [41].

The procedure of the present scheme can be summarized as follows:

1. At t^n , the interfacial distribution function and its associated spatial gradients are calculated by a second-order interpolation method, as done in a previous work [41].
2. At $t^{n+1/2}$, update the macroscopic fields at the cell interface based on Eqs. (24,25,26,27,5,6). Then, update the equilibrium distribution function of phonon/electron based on Eq. (3).

3. At $t^{n+1/2}$, update the electron/phonon distribution function at the cell interface based on Eqs. (20,21,22,23).
4. At t^{n+1} , update the macroscopic fields at the cell center based on Eqs. (14,15,5,6). Then, update the equilibrium distribution function of phonon/electron based on Eq. (3).
5. At t^{n+1} , update phonon/electron distribution function at the cell center based on Eqs. (12,13).

3. Numerical tests

The performance of the present scheme for electron-phonon coupling is validated by numerical tests in this part. Numerical results are compared with those predicted by typical two-temperature models (TTM), explicit discrete ordinate method (DOM) and discrete unified gas kinetic (DUGKS) in previous references [33]. In quasi-1D simulations, the Gauss–Legendre quadrature is used to discrete $\cos \theta \in [-1, 1]$ into N_θ points. In quasi-2D or 3D simulations, the Gauss–Legendre quadrature is also used to discretize the azimuthal angle $\varphi \in [0, \pi]$ into $N_\varphi/2$ points due to symmetry. All simulations were executed using a single core of AMD Ryzen 7 5800H with Radeon Graphics. The Knudsen number is defined as the ratio of the mean free path $\lambda = |\mathbf{v}| \tau$ to the characteristic length of the system, i.e., $\text{Kn} = \lambda/L$. The physical time step Δt is

$$\Delta t = \text{CFL} \times \frac{\{\Delta x, \Delta y\}_{min}}{\{|v_e|, |v_p|\}_{max}} \quad (28)$$

where $0 < \text{CFL} < 1$ is the Courant–Friedrichs–Lewy number. Without special statements, $\text{CFL}=0.40$.

3.1. Quasi-1D heat conduction

Quasi-1D cross-plane heat conduction in Au metal films with varying thicknesses is investigated. Isothermal boundary conditions are implemented for the left and right ends of the film with constant temperatures $T_L = T_0 + \Delta T$ and $T_R = T_0 - \Delta T$, respectively. Detailed thermophysical parameters of Au metals are shown below: electron mean free path $\lambda_e=33$ nm, phonon mean free path $\lambda_p=1.5$ nm, electron relaxation time $\tau_e=0.0243$ ps and phonon relaxation time $\tau_p=0.679$ ps. 40 discretized cells and $N_\theta=48$ discretized angles are used. The convergence is reach when

$$\epsilon = \frac{\sqrt{\sum_i (T_i^n - T_i^{n+1})^2}}{\sqrt{\sum_i (\Delta T)^2}} < 10^{-8} \quad (29)$$

The spatial distributions of the phonon temperature at various thicknesses are plotted in Fig. 1. A transition of the phonon temperature distribution from non-linear to near-linear is observed as the film thickness is increased from the nanometer to the micrometer scale, indicating a shift in the dominant heat conduction mechanism from the ballistic to diffusive. Specifically, pronounced nonlinearity is exhibited by the temperature curve when $L=100$ nm, which signifies the presence of significant ballistic transport effects in energy carriers. In contrast, a nearly linear distribution is approached by the temperature profile at $10 \mu\text{m}$, which is consistent with the description of Fourier's diffusion law, demonstrating the dominance of diffusion mechanisms at this scale. The reliable consistency of the present method with previous methods

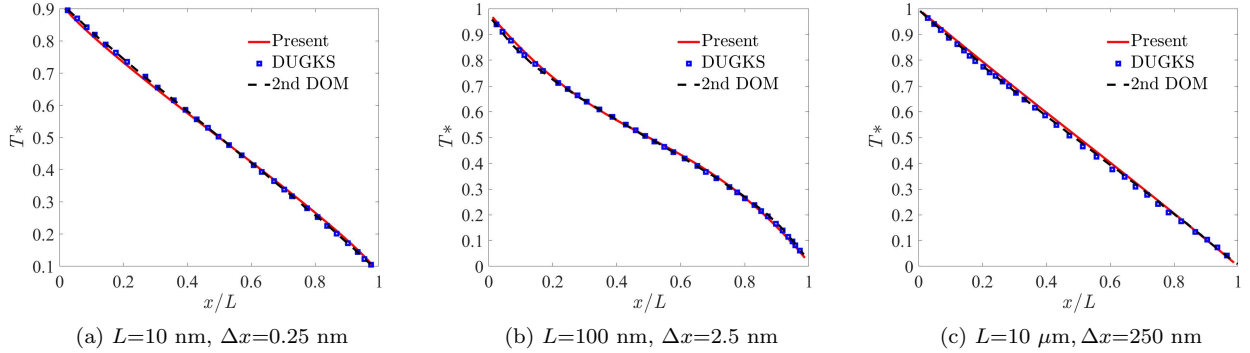


Figure 1: Spatial distributions of the phonon temperatures with different thickness L , where $T^* = (T - T_R)/(T_L - T_R)$.

across a broad range of scales, from ballistic to diffusive regime, is demonstrated, confirming its suitability for multiscale heat conduction analysis.

3.2. Transient thermal grating

Transient thermal grating technique is an advanced approach for measuring the thermal properties of nanomaterials [43, 44, 45]. A periodic temperature distribution, for instance of a sinusoidal or cosine shape,

$$T_e(x, t = 0) = T_{ref} + \Delta T \sin(2\pi x/L), \quad T_p(x, t = 0) = T_{ref}. \quad (30)$$

is achieved on the sample surface by the fundamental principle wherein optical interference fringes are generated by two coherent pump beams, where ΔT is the temperature amplitude, L is the spatial grating period length and the laser heating system initially only heats the electronic system. To simulate transient thermal phenomenon, 20-100 discretized cells and $N_\theta=8-100$ discretized angles are used. Periodic boundary conditions were applied to the left and right boundaries of single spatial grating period. Physical parameters of BTE in Au metals at 300 K and 25 K were obtained from previous reference.

The evolution of electron/phonon temperatures from nanometers to microns is systematically illustrated in Figs. 2 and 3 at normal or extremely low temperatures. It can be found that validation of the algorithm's accuracy is achieved through the close agreement of its results with those of the DUGKS across various scales. As demonstrated in Figs. 2a, 2c, 3a and 3d for the 100 nm scale, the predicted electron cooling rates, maximum phonon temperature increases, and their onset times are found to be nearly identical between the two methods. The curves are shown to be in substantial agreement at other larger scales. Furthermore, it can be seen that at lower temperatures, the increase in the hot carrier mean free path leads to the time required for electron-phonon thermal equilibrium to be shortened, thereby enhancing the non-equilibrium ballistic effect. It is indicated that the strength of the non-equilibrium transport phenomenon is significantly influenced by temperature.

Significant deviations of the traditional TTM from present or DUGKS' results are exhibited at the nanoscale, while convergence toward agreement is observed at larger scales. For $L=100$ nm (Figs. 2a, 2c,

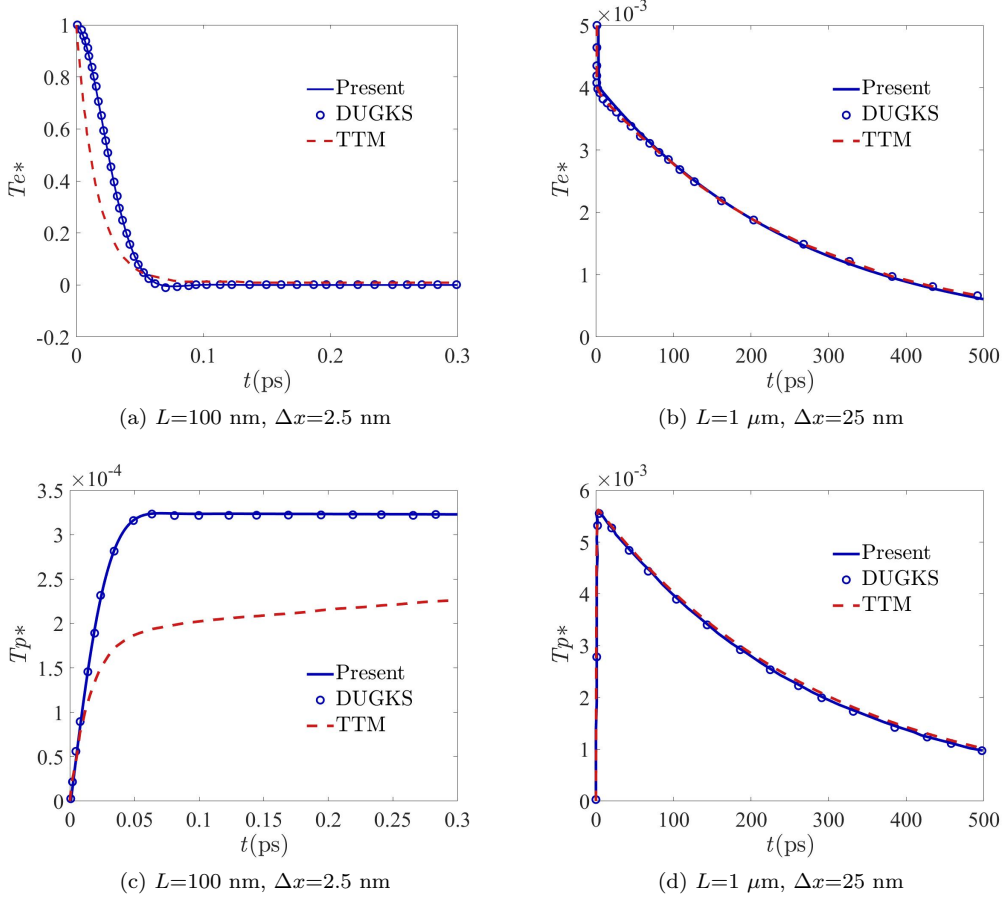


Figure 2: Time-dependent electron and phonon temperatures at $x = L/4$ with different L , where $T_{ref} = 300$ K, $\Delta T = 1$ K, $T_e^* = (T_e - T_{ref}) / \Delta T$, $T_p^* = (T_p - T_{ref}) / \Delta T$. The data predicted by the DUGKS and TTM is obtained from previous reference [33].

3a and 3d), both the electron cooling rate and the peak phonon temperature are underestimated by TTM; as the scale is increased to 1 μm (Figs. 2b, 2d, 3b and 3e), the deviation is reduced, though systematically low predictions are still maintained by TTM; at the 10 μm (Figs. 3c and 3f), consistency is largely achieved among all three methods. This indicates that TTM is applicable in regions where macroscopic diffusion is dominant, yet its limitations are revealed in ultra-fast non-equilibrium processes at the nanoscale.

The energy transfer process is visualized through a comparison of the electron and phonon temperature curves. A significantly shorter characteristic time is exhibited by electron temperature changes (cooling) compared to phonon temperature changes (heating). At small scales, the process is dominated by extremely rapid electron-phonon coupling, characterized by a plunge in electron temperature within sub-picoseconds and a sharp response in phonon temperature (Figs. 2a, 2c, 3a and 3d). At the mesoscale, both temperatures are observed to evolve slowly over tens of picoseconds, showing distinct coupled relaxation characteristics (Figs. 2b, 2d, 3b and 3e). At the macroscale, temperature changes occur very slowly, approaching classical diffusion behavior (Figs. 3c and 3f). The complete relaxation chain following TTG excitation is revealed:

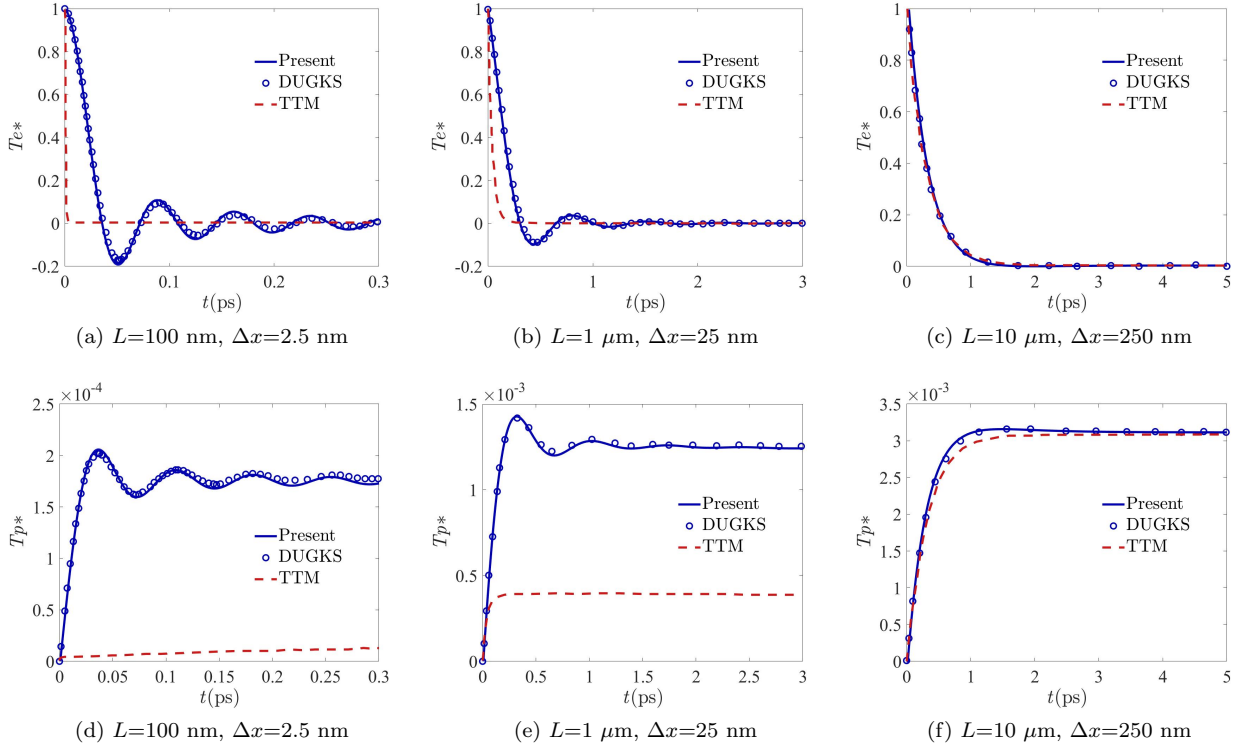


Figure 3: Time-dependent electron and phonon temperatures at $x = L/4$ with different L , where $T_{ref} = 25$ K, $\Delta T = 1$ K, $T_e^* = (T_e - T_{ref}) / \Delta T$, $T_p^* = (T_p - T_{ref}) / \Delta T$. The data predicted by the DUGKS and TTM is obtained from previous reference [33].

energy is initially deposited in the electron subsystem, then transferred to the phonon subsystem via electron-phonon coupling, until thermal equilibrium is finally reached.

In summary, the precise capture of heat transport behavior across multiple scales is achieved by the present algorithm. A high level of agreement with the results from the DUGKS is shown, while superior performance over the traditional TTM in modeling nanoscale ultra-fast non-equilibrium thermal processes is exhibited.

4. Conclusion

A semi-implicit Lax-Wendroff kinetic scheme is developed, whereby a unified computational framework is provided for the thermal simulation of coupled electron-phonon transport across ballistic and diffusive regimes. The distinctive feature of this method is that it integrates the physical evolution information of heat carriers into the numerical modeling process. Specifically, the finite difference method is employed to resolve the kinetic model of electron-phonon coupling again when reconstructing the interfacial distribution function. Consequently, the particle migration, scattering and electron-phonon coupling processes are coupled within a single time step, which successfully breaks the temporal and spatial constraints imposed by relaxation time and mean free path without the loss of solution accuracy. The robustness and computational efficiency of

this methodology for multiscale thermal conduction are validated through numerical tests. It is anticipated that this work will contribute to a more profound understanding of electron–phonon interactions and provide a refined instrument for thermal management within next-generation microelectronic devices.

Acknowledgments

C. Z. acknowledges the support of the National Natural Science Foundation of China (52506078) and Zhejiang Provincial Natural Science Foundation of China under Grant No.LMS26E060012. C. Z. acknowledges the members of online WeChat Group: Device Simulation Happy Exchange Group, and acknowledges Beijing PARATERA Tech CO., Ltd. for the HPC resources. H. L. acknowledges the support of the National Natural Science Foundation of China (12572285).

References

- [1] M. M. Waldrop, The chips are down for Moore’s law, *Nature News* 530 (2016) 144. URL: <http://www.nature.com/news/the-chips-are-down-for-moore-s-law-1.19338>. doi:10.1038/530144a.
- [2] Q. Zhang, Y. Zhang, Y. Luo, H. Yin, New structure transistors for advanced technology node cmos ics, *National Science Review* 11 (2024) nwae008. URL: <https://doi.org/10.1093/nsr/nwae008>. doi:10.1093/nsr/nwae008.
- [3] M. A. Stettler, S. M. Cea, S. Hasan, L. Jiang, P. H. Keys, C. D. Landon, P. Marepalli, D. Pantuso, C. E. Weber, Industrial TCAD: Modeling atoms to chips, *IEEE Transactions on Electron Devices* 68 (2021) 5350–5357. doi:10.1109/TED.2021.3076976.
- [4] M. Kaviany, *Heat transfer physics*, Cambridge University Press, 2008. URL: <https://doi.org/10.1017/CBO9780511754586>. doi:10.1017/CBO9780511754586.
- [5] E. Pop, R. W. Dutton, K. E. Goodson, Analytic band monte carlo model for electron transport in si including acoustic and optical phonon dispersion, *J. Appl. Phys.* 96 (2004) 4998–5005. URL: <http://aip.scitation.org/doi/10.1063/1.1788838>. doi:10.1063/1.1788838.
- [6] V. Chiloyan, S. Huberman, A. A. Maznev, K. A. Nelson, G. Chen, Thermal transport exceeding bulk heat conduction due to nonthermal micro/nanoscale phonon populations, *Appl. Phys. Lett.* 116 (2020) 163102. URL: <https://doi.org/10.1063/1.5139069>. doi:10.1063/1.5139069.
- [7] E. Pop, Energy dissipation and transport in nanoscale devices, *Nano Res.* 3 (2010) 147–169. URL: <https://doi.org/10.1007/s12274-010-1019-z>. doi:10.1007/s12274-010-1019-z.
- [8] B. Cao, Thermal design automation (tda) for multiscale thermal management of electronics, *Journal of Applied Physics* 138 (2025) 180901. URL: <https://doi.org/10.1063/5.0288828>. doi:10.1063/5.0288828.

[9] G. Chen, Nanoscale energy transport and conversion: A parallel treatment of electrons, molecules, phonons, and photons, Oxford University Press, 2005. URL: <https://global.oup.com/ushe/product/nanoscale-energy-transport-and-conversion-9780195159424?cc=cn&lang=en&>.

[10] J. M. Ziman, Electrons and phonons: the theory of transport phenomena in solids, Oxford University Press, 1960. URL: <https://global.oup.com/academic/product/electrons-and-phonons-9780198507796?cc=cn&lang=en&>.

[11] F. Giustino, Electron-phonon interactions from first principles, *Rev. Mod. Phys.* 89 (2017) 015003. URL: <https://link.aps.org/doi/10.1103/RevModPhys.89.015003>. doi:10.1103/RevModPhys.89.015003.

[12] S. Ono, Thermalization in simple metals: Role of electron-phonon and phonon-phonon scattering, *Phys. Rev. B* 97 (2018) 054310. URL: <https://link.aps.org/doi/10.1103/PhysRevB.97.054310>. doi:10.1103/PhysRevB.97.054310.

[13] Z. Lu, A. Vallabhaneni, B. Cao, X. Ruan, Phonon branch-resolved electron-phonon coupling and the multitemperature model, *Phys. Rev. B* 98 (2018) 134309. URL: <https://link.aps.org/doi/10.1103/PhysRevB.98.134309>. doi:10.1103/PhysRevB.98.134309.

[14] A. K. Vallabhaneni, D. Singh, H. Bao, J. Murthy, X. Ruan, Reliability of Raman measurements of thermal conductivity of single-layer graphene due to selective electron-phonon coupling: A first-principles study, *Phys. Rev. B* 93 (2016) 125432. URL: <https://link.aps.org/doi/10.1103/PhysRevB.93.125432>. doi:10.1103/PhysRevB.93.125432.

[15] P. B. Allen, Theory of thermal relaxation of electrons in metals, *Phys. Rev. Lett.* 59 (1987) 1460–1463. URL: <https://link.aps.org/doi/10.1103/PhysRevLett.59.1460>. doi:10.1103/PhysRevLett.59.1460.

[16] E. Carpene, Ultrafast laser irradiation of metals: Beyond the two-temperature model, *Phys. Rev. B* 74 (2006) 024301. URL: <https://link.aps.org/doi/10.1103/PhysRevB.74.024301>. doi:10.1103/PhysRevB.74.024301.

[17] R. W. Schoenlein, W. Z. Lin, J. G. Fujimoto, G. L. Eesley, Femtosecond studies of nonequilibrium electronic processes in metals, *Phys. Rev. Lett.* 58 (1987) 1680–1683. URL: <https://link.aps.org/doi/10.1103/PhysRevLett.58.1680>. doi:10.1103/PhysRevLett.58.1680.

[18] R. H. M. Groeneveld, R. Sprik, A. Lagendijk, Effect of a nonthermal electron distribution on the electron-phonon energy relaxation process in noble metals, *Phys. Rev. B* 45 (1992) 5079–5082. URL: <https://link.aps.org/doi/10.1103/PhysRevB.45.5079>. doi:10.1103/PhysRevB.45.5079.

- [19] F. Caruso, D. Novko, Ultrafast dynamics of electrons and phonons: from the two-temperature model to the time-dependent boltzmann equation, *Advances in Physics: X* 7 (2022) 2095925. URL: <https://doi.org/10.1080/23746149.2022.2095925>. doi:10.1080/23746149.2022.2095925.
- [20] L. Waldecker, R. Bertoni, R. Ernstorfer, J. Vorberger, Electron-phonon coupling and energy flow in a simple metal beyond the two-temperature approximation, *Phys. Rev. X* 6 (2016) 021003. URL: <https://link.aps.org/doi/10.1103/PhysRevX.6.021003>. doi:10.1103/PhysRevX.6.021003.
- [21] T. Qiu, C. Tien, Femtosecond laser heating of multi-layer metals—i. analysis, *Int. J. Heat Mass Transfer* 37 (1994) 2789–2797. URL: <https://www.sciencedirect.com/science/article/pii/0017931094903964>. doi:[https://doi.org/10.1016/0017-9310\(94\)90396-4](https://doi.org/10.1016/0017-9310(94)90396-4).
- [22] S. I. Anisimov, B. L. Kapeliovich, T. L. Perelman, Electron emission from metal surfaces exposed to ultrashort laser pulses, *Sov. Phys.-JETP* 39 (1974) 375–377.
- [23] R. Wang, H. Zobeiri, Y. Xie, X. Wang, X. Zhang, Y. Yue, Distinguishing optical and acoustic phonon temperatures and their energy coupling factor under photon excitation in nm 2d materials, *Advanced Science* 7 (2020) 2000097. URL: <https://onlinelibrary.wiley.com/doi/abs/10.1002/advs.202000097>. doi:<https://doi.org/10.1002/advs.202000097>.
- [24] H. Zobeiri, N. Hunter, R. Wang, T. Wang, X. Wang, Direct characterization of thermal nonequilibrium between optical and acoustic phonons in graphene paper under photon excitation, *Advanced Science* 8 (2021) 2004712. URL: <https://onlinelibrary.wiley.com/doi/abs/10.1002/advs.202004712>. doi:<https://doi.org/10.1002/advs.202004712>.
- [25] S. Sullivan, A. Vallabhaneni, I. Kholmanov, X. Ruan, J. Murthy, L. Shi, Optical generation and detection of local nonequilibrium phonons in suspended graphene, *Nano Letters* 17 (2017) 2049–2056. URL: <https://doi.org/10.1021/acs.nanolett.7b00110>. doi:10.1021/acs.nanolett.7b00110.
- [26] D. D. Joseph, L. Preziosi, Heat waves, *Rev. Mod. Phys.* 61 (1989) 41–73. URL: <https://link.aps.org/doi/10.1103/RevModPhys.61.41>. doi:10.1103/RevModPhys.61.41.
- [27] J. Chen, D. Tzou, J. Beraun, A semiclassical two-temperature model for ultrafast laser heating, *Int. J. Heat Mass Transfer* 49 (2006) 307–316. URL: <https://www.sciencedirect.com/science/article/pii/S001793100500445X>. doi:<https://doi.org/10.1016/j.ijheatmasstransfer.2005.06.022>.
- [28] A. Pattamatta, C. K. Madnia, Modeling Electron-Phonon Nonequilibrium in Gold Films Using Boltzmann Transport Model, *J. Heat Transf.* 131 (2009) 082401. URL: <https://doi.org/10.1115/1.3111258>.

[29] W. Miao, M. Wang, Nonequilibrium effects on the electron-phonon coupling constant in metals, Phys. Rev. B 103 (2021) 125412. URL: <https://link.aps.org/doi/10.1103/PhysRevB.103.125412>. doi:10.1103/PhysRevB.103.125412.

[30] X. Tong, M. Bernardi, Toward precise simulations of the coupled ultrafast dynamics of electrons and atomic vibrations in materials, Phys. Rev. Research 3 (2021) 023072. URL: <https://link.aps.org/doi/10.1103/PhysRevResearch.3.023072>. doi:10.1103/PhysRevResearch.3.023072.

[31] Y. Wang, Z. Lu, A. K. Roy, X. Ruan, Effect of interlayer on interfacial thermal transport and hot electron cooling in metal-dielectric systems: An electron-phonon coupling perspective, J. Appl. Phys. 119 (2016) 065103. URL: <https://doi.org/10.1063/1.4941347>. doi:10.1063/1.4941347.

[32] C. Zhang, H. Rezgui, M. Lian, H. Liang, Non-equilibrium transport and phonon branch-resolved size effects based on a multi-temperature kinetic model, Materials Today Physics 59 (2025) 101893. URL: <https://www.sciencedirect.com/science/article/pii/S2542529325002494>. doi:<https://doi.org/10.1016/j.mtphys.2025.101893>.

[33] C. Zhang, R. Guo, M. Lian, J. Shiomi, Electron-phonon coupling and non-equilibrium thermal conduction in ultra-fast heating systems, Applied Thermal Engineering 249 (2024) 123379. URL: <https://www.sciencedirect.com/science/article/pii/S1359431124010470>. doi:<https://doi.org/10.1016/j.aplthermaleng.2024.123379>.

[34] Z. Guo, K. Xu, Progress of discrete unified gas-kinetic scheme for multiscale flows, Adva. Aerodyn. 3 (2021) 6. URL: <https://doi.org/10.1186/s42774-020-00058-3>. doi:10.1186/s42774-020-00058-3.

[35] S. Succi, I. V. Karlin, H. Chen, Colloquium: Role of the h theorem in lattice boltzmann hydrodynamic simulations, Rev. Mod. Phys. 74 (2002) 1203–1220. URL: <https://link.aps.org/doi/10.1103/RevModPhys.74.1203>. doi:10.1103/RevModPhys.74.1203.

[36] W. Miao, M. Wang, Importance of electron-phonon coupling in thermal transport in metal/semiconductor multilayer films, Int. J. Heat Mass Transfer 200 (2023) 123538. URL: <https://www.sciencedirect.com/science/article/pii/S0017931022010079>. doi:<https://doi.org/10.1016/j.ijheatmasstransfer.2022.123538>.

[37] A. Muthukunnil Joseph, B.-Y. Cao, An electron-phonon monte carlo study on thermal transport in GaN, Int. J. Therm. Sci. 181 (2022) 107742. URL: <https://www.sciencedirect.com/science/article/pii/S1290072922002757>. doi:<https://doi.org/10.1016/j.ijthermalsci.2022.107742>.

[38] F. Filbet, S. Jin, A class of asymptotic-preserving schemes for kinetic equations and related problems with stiff sources, *J. Comput. Phys.* 229 (2010) 7625 – 7648. URL: <http://www.sciencedirect.com/science/article/pii/S0021999110003323>. doi:10.1016/j.jcp.2010.06.017.

[39] Z. Guo, J. Li, K. Xu, Unified preserving properties of kinetic schemes, *Phys. Rev. E* 107 (2023) 025301. URL: <https://link.aps.org/doi/10.1103/PhysRevE.107.025301>. doi:10.1103/PhysRevE.107.025301.

[40] G. A. Bird, *Molecular Gas Dynamics And The Direct Simulation Of Gas Flows*, Oxford University Press, 1994. URL: <https://doi.org/10.1093/oso/9780198561958.001.0001>. doi:10.1093/oso/9780198561958.001.0001.

[41] S. Peng, S. Chen, H. Liang, C. Zhang, Semi-implicit lax-wendroff kinetic scheme for multi-scale phonon transport, *Computers & Mathematics with Applications* 187 (2025) 72–84. URL: <https://www.sciencedirect.com/science/article/pii/S0898122125001130>. doi:<https://doi.org/10.1016/j.camwa.2025.03.019>.

[42] S. Chen, Z. Guo, K. Xu, Z. Li, Semi-implicit Richtmyer (Lax-Wendroff) scheme for kinetic equation with relaxation term, *ResearchGate* (2022). URL: https://www.researchgate.net/publication/365195373_Semi-implicit_Richtmyer_Lax-Wendroff_scheme_for_kinetic_equation_with_relaxation_term. doi:10.13140/RG.2.2.33938.94403.

[43] K. C. Collins, A. A. Maznev, Z. Tian, K. Esfarjani, K. A. Nelson, G. Chen, Non-diffusive relaxation of a transient thermal grating analyzed with the Boltzmann transport equation, *J. Appl. Phys.* 114 (2013) 104302. URL: <https://aip.scitation.org/doi/10.1063/1.4820572>. doi:10.1063/1.4820572.

[44] A. A. Maznev, J. A. Johnson, K. A. Nelson, Non-equilibrium transient thermal grating relaxation in metal, *J. Appl. Phys.* 109 (2011) 073517. URL: <https://doi.org/10.1063/1.3569731>. doi:10.1063/1.3569731.

[45] Y. Sivan, M. Spector, Ultrafast dynamics of optically induced heat grating in metals, *ACS Photonics* 7 (2020) 1271–1279. URL: <https://doi.org/10.1021/acsphotonics.0c00224>. doi:10.1021/acsphotonics.0c00224.